⌘ *Author's Choice*

THE JOURNAL OF BIOLOGICAL CHEMISTRY VOL. 285, NO. 44, pp. 33764–33770, October 29, 2010

Implications for Collagen Binding from the Crystallographic Structure of Fibronectin ^{6}FnI$^{1-2}$FnII^{7}FnI[S]

Received for publication, May 3, 2010, and in revised form, August 5, 2010 Published, JBC Papers in Press, August 24, 2010, DOI 10.1074/jbc.M110.139394

Michèle C. Erat[‡1], Ulrich Schwarz-Linek[§], Andrew R. Pickford[¶2], Richard W. Farndale[‖3], Iain D. Campbell[‡2], and Ioannis Vakonakis[‡4]

From the [‡]Department of Biochemistry, University of Oxford, Oxford OX1 3QU, the [§]Biomedical Sciences Research Complex, University of St. Andrews, St. Andrews, Fife, KY16 9ST, Scotland, the [¶]School of Biological Sciences, University of Portsmouth, Portsmouth PO1 2DY, and the [‖]Department of Biochemistry, University of Cambridge, Cambridge CB2 1QW, United Kingdom

Collagen and fibronectin (FN) are two abundant and essential components of the vertebrate extracellular matrix; they interact directly with cellular receptors and affect cell adhesion and migration. Past studies identified a FN fragment comprising six modules, ^{6}FnI$^{1-2}$FnII$^{7-9}$FnI, and termed the gelatin binding domain (GBD) as responsible for collagen interaction. Recently, we showed that the GBD binds tightly to a specific site within type I collagen and determined the structure of domains $^{8-9}$FnI in complex with a peptide from that site. Here, we present the crystallographic structure of domains ^{6}FnI$^{1-2}$FnII^{7}FnI, which form a compact, globular unit through interdomain interactions. Analysis of NMR titrations with single-stranded collagen peptides reveals a dominant collagen interaction surface on domains ^{2}FnII and ^{7}FnI; a similar surface appears involved in interactions with triple-helical peptides. Models of the complete GBD, based on the new structure and the $^{8-9}$FnI·collagen complex show a continuous putative collagen binding surface. We explore the implications of this model using long collagen peptides and discuss our findings in the context of FN interactions with collagen fibrils.

Collagen fibrils are the basis of vertebrate tissue, and their formation is vital for cell differentiation, cell migration, and embryonic development (1). The most abundant form, collagen type I, consists of two chains of α_1 and one of α_2 that intertwine to create right-handed triple helices, which then assemble to make microfibrils and fibers (2, 3). Fibril formation of type I collagen *in vivo* requires integrin receptors and fibronectin (FN),[5] a large glycoprotein composed of three domain classes, FnI, FnII, and FnIII (4, 5). FN forms fibrils in the extracellular matrix and interacts with denatured collagen (gelatin) or isolated collagen chains. The interaction site on FN is the gelatin binding domain (GBD), consisting of four FnI and two FnII modules (^{6}FnI$^{1-2}$FnII$^{7-9}$FnI) (6). The first structure of a FN·collagen complex, a $^{8-9}$FnI fragment together with a single-stranded collagen peptide was recently determined (7). This structure and subsequent biophysical analysis suggested that $^{8-9}$FnI preferentially binds to unwound collagen. Interestingly, the proposed binding site for FN on collagen I coincides with the cleavage site for metalloproteinase 1, the so-called collagenase site (8–10). This site is hydrophobic and relatively low in proline and hydroxyproline residues, rendering the triple helix unstable at physiological temperature (11). Although these results offered some answers on FN·collagen binding, the role of the remaining four domains in GBD was unclear. The solution NMR structure of ^{6}FnI$^{1-2}$FnII (12) suggested that ^{1}FnII reorients flexibly with respect to ^{6}FnI-^{2}FnII. However, ^{6}FnI$^{1-2}$FnII shows substantially decreased binding to gelatin (13) and collagen peptides (14) compared with ^{6}FnI$^{1-2}$FnII^{7}FnI, implying a significant role for the ^{7}FnI domain in this interaction. Here, we present the crystallographic structure of the ^{6}FnI$^{1-2}$FnII^{7}FnI fragment at a resolution of 3.0 Å. We compare this new structure with the previous solution structure of ^{6}FnI$^{1-2}$FnII and show that ^{1}FnII and ^{2}FnII jointly form an interface for ^{7}FnI; the presence of this interface in solution is supported by analysis of the NMR chemical shifts of these fragments. NMR titrations with single-stranded as well as triple-helical peptides from the collagenase site show that a unique binding surface, involving domains ^{2}FnII and ^{7}FnI, is important for collagen binding. Together with previously published data (7), we now offer a model for the complete GBD which suggests that the two GBD subfragments bind collagen in a concerted fashion.

EXPERIMENTAL PROCEDURES

Protein Expression, Purification, and Crystallization—A gene fragment, encoding FN residues 305–515, corresponding to domains ^{6}FnI$^{1-2}$FnII^{7}FnI, and bearing a single amino acid substitution (H307D) and a C-terminal His_6 tag (GTKHHHHHH) was integrated in *Pichia pastoris* in a manner analogous to that previously described (15). The H307D substitution does not affect the binding of ^{6}FnI$^{1-2}$FnII^{7}FnI to gelatin-Sepharose columns (data not shown) but increases the solubility of this fragment under physiological pH conditions significantly. Cells

⌘ *Author's Choice*—Final version full access.

[S] The on-line version of this article (available at http://www.jbc.org) contains supplemental Figs. 1–6 and Table 1.

The atomic coordinates and structure factors (code 3MQL) have been deposited in the Protein Data Bank, Research Collaboratory for Structural Bioinformatics, Rutgers University, New Brunswick, NJ (http://www.rcsb.org/).

The NMR chemical shifts have been deposited in the BioMagResBank, www.bmrb.wisc.edu (accession no. 16841).

[1] Supported by EC Marie Curie Fellowship FP7.

[2] Supported by the Biotechnology and Biological Sciences Research Council.

[3] Supported by the Medical Research Council.

[4] Supported by the Wellcome Trust Career Development fellowship program. To whom correspondence should be addressed: Dept. of Biochemistry, South Parks Road, Oxford OX1 3QU, United Kingdom. Tel.: 44 1865 613219; Fax: 44 1865 613298; E-mail: ioannis.vakonakis@bioch.ox.ac.uk.

[5] The abbreviations used are: FN, fibronectin; α_1(I)/(II), collagen type I/II α_1 chain; FnI/II/III, FN type I/II/III domains; GBD, gelatin binding domain; ITC, isothermal titration calorimetry.

were grown under high density fermentation conditions, using a minimal phosphate medium at pH 3.25 and 30 °C; protein expression was induced by the addition of methanol over the course of 5–7 days. ^{6}FnI$^{1-2}$FnII^{7}FnI was purified from the expression media by metal affinity chromatography, and the *N*-linked glycan at Asn^{430} was truncated by endoglycosidase H treatment, leaving a single *N*-acetylglucosamine at this site. The protein was further purified by reverse phase HPLC, lyophilized, and finally run on a Sephadex G-75 size exclusion column equilibrated in a 100 mM NaCl, 10 mM HEPES, pH 7.2, buffer. ^{6}FnI$^{1-2}$FnII^{7}FnI was concentrated in this buffer to ~25 mg/ml.

Crystallization drops were formed by 1:1 mixtures of protein in the final purification buffer at 17.5 mg/ml concentration, and a 0.2 M $(NH_4)H_2PO_4$, 0.1 M Tris-Cl, pH 8.5, 50% v/v 2-methyl-2,4-pentanediol solution. Sitting-drop vapor diffusion was employed in 96-well plates, with drop volumes varying between 200 and 400 nl. ^{6}FnI$^{1-2}$FnII^{7}FnI crystals of lens-like appearance and ~200 μm in the longest axis developed after 6–8 weeks at 20 °C. Crystals were cryoprotected by brief immersion in crystallization mother liquor and frozen in a nitrogen cryostream at 100 K.

X-ray Data Collection and Processing, Structure Determination—Data were collected under cryogenic conditions at the PXIII macromolecular crystallography beamline at the Swiss Light Source (Villigen, Switzerland). Reflection data were indexed by LABELIT (16), refined and integrated in XDS (17), and merged by SCALA (18). The Laue group and space group were suggested by POINTLESS (18) from the unmerged data, and data quality was assessed by PHENIX.xtriage (19) (supplemental Table 1).

Initial structure determination was performed by molecular replacement using PHASER (20) and superimposed ensembles of FnI- and FnII-type modules of known crystallographic structures. Iterative cycles of model building in COOT (21) and refinement using PHENIX.refine (19) with TLS restraints (one chain) resulted in a final model with satisfactory R_{work}/R_{free} and MolProbity (22) statistics (supplemental Table 1).

NMR Data Collection and Assignments—Details of the ^{6}FnI$^{1-2}$FnII^{7}FnI sample preparation for NMR experiments as well as the titration with collagen peptides were described earlier (7). The triple-helical α_1(II) Gly^{775}-Ser^{801} peptide was synthesized and verified as described (23, 24) and was then allowed to anneal for 24 h at 4 °C at high concentrations (>1 mM) prior to use. Sequence-specific chemical shift assignments were performed using a uniformly ^{13}C^{15}N-enriched ^{6}FnI$^{1-2}$FnII^{7}FnI sample of ~1 mM concentration in a 20 mM Na_2HPO_4, pH 7.2, buffer at 37 °C. Home-built or Bruker Avance II spectrometers were used for a combination of standard through-bond triple-resonance experiments (25) supplemented by through-bond experiments for assignments of aromatic side chains (26).

Circular Dichroism (CD) Spectroscopy—CD spectra were collected using Jasco J-720 or AppliedPhotphysics Chirascan spectropolarimeters with a 0.1-cm path length. Peptide samples of 50 μM (α_1(II) Gly^{775}-Ser^{801}) or 300 μM (α_1(I) Gly^{778}-Arg^{816}) concentration in an aqueous buffer containing 150 mM NaCl, 20 mM Na_2HPO_4, pH 7.4, were used.

Isothermal Titration Calorimetry (ITC)—Recombinant $^{8-9}$FnI and GBD were prepared as described earlier (7). The α_1(I) Gly^{778}-Arg^{816} peptide was purchased from GL Biochem (Shanghai) as HPLC-purified, lyophilized powder. Protein concentration was established by UV absorbance at 280 nm, and peptide concentration was initially estimated from dry weight. Protein solutions were dialyzed overnight against 150 mM NaCl, 20 mM Na_2HPO_4, pH 7.2. The pH of peptide solutions was adjusted with 1 M NaOH to match this buffer. ITC experiments (VP-ITC; MicroCal) were performed as follows: one injection of 2 μl followed by 44 injections of 5 μl at 0.5 μl/s. The stirring speed was 307 rpm; the delay between the injections was 210 s. To take into account heats of dilution, blank titrations were performed by injecting peptide solution into buffer, and the averaged heat of dilution was subtracted from the main experiment. Raw data were processed and fitted to a one-site model using MicroCal Origin software.

Data Deposition—Amino acid composition and numbering for FN fragments correspond to UniProt entry B7ZLF0. α_1(I) and α_1(II) numbering (accession numbers P02452 and P02458, respectively) begins at the estimated start of the helical region. O in peptide sequences denotes 4-hydroxyproline. Structural analysis was performed, and figures were prepared using PyMOL (27). Interdomain interactions were analyzed with the PISA service from the European Bioinformatics Institute (28). Structural data have been deposited in the Protein Data Bank under accession number 3MQL, and NMR chemical shift assignments are available in the BioMagResBank under accession number 16841.

RESULTS

Structure of ^{6}FnI$^{1-2}$FnII^{7}FnI—A FN fragment spanning domains ^{6}FnI$^{1-2}$FnII^{7}FnI crystallized using the sitting-drop vapor diffusion method as described under "Experimental Procedures." Lens-like birefringent objects grew slowly out of initial light precipitate over the course of ~2 months at 20 °C. Despite the lack of well defined edges, these objects were crystalline in nature and diffracted to ~3.5 Å resolution in synchrotron x-ray sources. Screening around the initial crystallization conditions or use of additives did not improve the morphology of these crystals; however, it was possible to collect a complete 3.0 Å dataset (supplemental Table 1) by screening different crystals from the original conditions. The Matthews coefficient strongly suggested a single ^{6}FnI$^{1-2}$FnII^{7}FnI molecule/asymmetric unit, and the structure was solved by molecular replacement using two copies of FnI- and FnII-type structural ensembles for a total of four search objects. The initial molecular replacement map was of sufficient quality to allow tracing of interdomain linkers and to establish domain identity and connectivity.

All individual ^{6}FnI$^{1-2}$FnII^{7}FnI domains adopt canonical structures (12, 29), a result anticipated based on chemical shift index analysis (30) of this fragment in solution. FnI-type domains form a β-sandwich with antiparallel two-stranded and three-stranded β-sheets. FnII-type domains are characterized by extensive loop segments and only two short antiparallel two-stranded sheets. Both FnI- and FnII-type domains feature two disulfide bridges that contribute substantially to these domain folds.

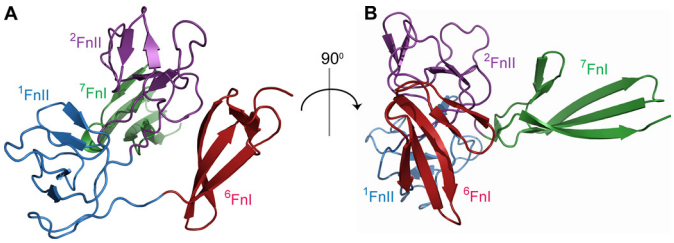

FIGURE 1. *A*, crystal structure of ^{6}FnI$^{1-2}$FnII^{7}FnI shows domain ^{6}FnI packing against $^{1-2}$FnII to form a compact triagonal shape. *B*, ^{7}FnI, in contrast, protrudes at an approximately 90° angle, presenting a large interface for potential interaction partners. The domains are colored individually: ^{6}FnI, *red*; ^{1}FnII, *blue*; ^{2}FnII, *purple*; and ^{7}FnI, *green*.

In contrast to common beads-on-string models of multidomain proteins (31), the crystallographic structure of ^{6}FnI$^{1-2}$FnII^{7}FnI adopts a pyramidal shape. As shown in Fig. 1*A* ^{6}FnI$^{1-2}$FnII forms an approximately equilateral triangle with sides of ~ 35 Å. From this base, ^{7}FnI projects out by ~38 Å (Fig. 1*B*) and forms extensive hydrogen-bonding interactions with a ^{7}FnI domain from a crystallographic 2-fold symmetry-related molecule. Other crystal contacts include further β-sheet extensions through ^{7}FnI-^{7}FnI and ^{6}FnI-^{6}FnI interactions; however, it should be noted that similar extensions are common among crystallographic structures of FnI-type domains (29, 32). No evidence of protein oligomerization was apparent in solution NMR experiments even at sample concentrations of >1 mM (data not shown).

The compact ^{6}FnI$^{1-2}$FnII^{7}FnI conformation is maintained through interdomain interactions that show a remarkable degree of conservation (supplemental Fig. 1). ^{6}FnI interacts with ^{2}FnII in a manner essentially identical to that observed in the solution ^{6}FnI$^{1-2}$FnII structure (12), burying ~395 Å^2 of solvent-accessible surface area (Fig. 2*A*). The C$^{\alpha}$ root mean square deviation for ^{6}FnI·^{2}FnII between the solution structure and our crystallographic model is only 1.7 Å, whereas the individual domains differ by 1.0 and 1.1 Å for ^{6}FnI and ^{2}FnII, respectively. Residues 314–323 of ^{6}FnI, and 414–421 and 448–449 of ^{2}FnII are primarily involved in forming the interface, with significant contributions from Met^{320}, Ser^{415}, Ala^{418}, Leu^{419}, Thr^{448}, and Thr^{449} (Fig. 2*A*).

The solution structure of ^{6}FnI$^{1-2}$FnII featured a well defined ^{1}FnII domain which was, however, mobile in relation to the ^{6}FnI·^{2}FnII complex (12). In contrast, our crystallographic model shows the formation of a ^{1}FnII-^{2}FnII interface (Fig. 2*B*) burying ~330 Å^2. ^{1}FnII rotates and translates toward ^{2}FnII and ^{7}FnI (Fig. 3, *A* and *B*, and below); this motion places ^{1}FnII outside the ensemble of conformations shown in the solution structure of ^{6}FnI$^{1-2}$FnII. The ^{1}FnII-^{2}FnII interface involves primarily Tyr^{372}, Val^{408}, and Pro^{462} as well as long range hydrogen bonds between Val^{315} O′-Asn^{416} N$^{\delta 2}$, Gln^{321} O′-Leu^{419} N, and Tyr^{316} O$^{\eta}$-Asn^{416} O′. In addition, ^{1}FnII helps to structure the relatively long linker (residues 461–468) connecting ^{2}FnII and ^{7}FnI, which in turn stabilizes the ^{7}FnI conformation relative to the remaining domains. ^{7}FnI interacts with both ^{1}FnII and ^{2}FnII across an interface burying ~390 Å^2 of solvent-accessible surface area (Fig. 2*C*). Residues Thr^{365}, Ser^{390}, Asn^{391}, Met^{463}, Ala^{464}, His^{466}, Ile^{469}, and Gly^{502} are involved in hydrophobic burial and hydrogen bonding interactions, whereas Arg^{479} and Ile^{480} help anchor ^{7}FnI to the structured ^{2}FnII-^{7}FnI linker (Fig. 2*C*).

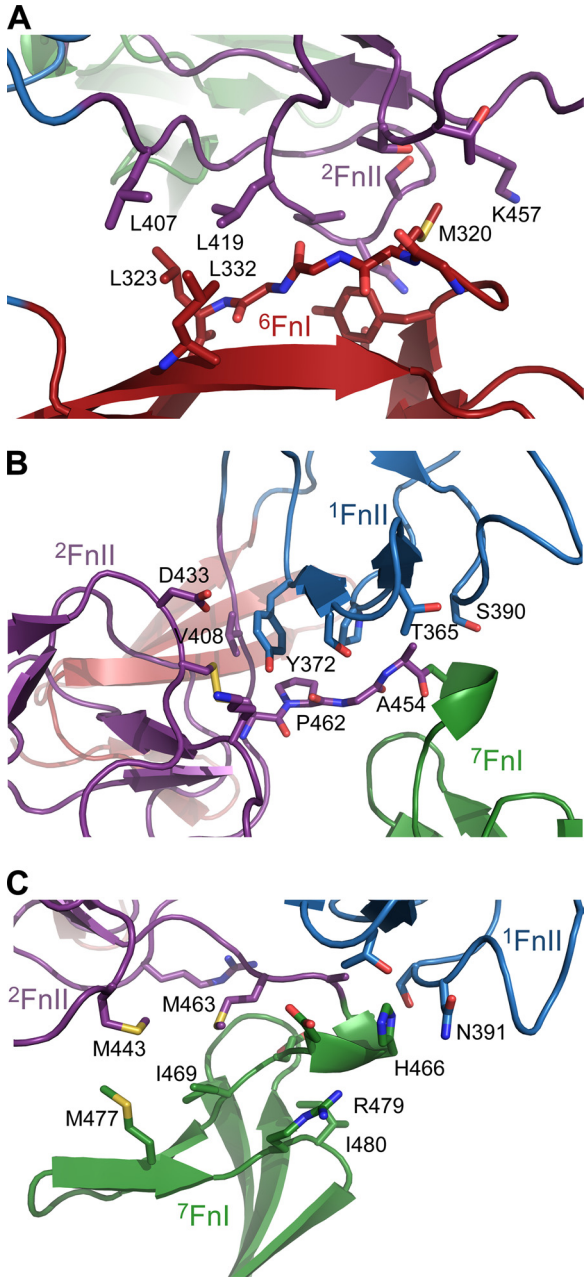

FIGURE 2. **Prominent domain-domain contacts involving ^{6}FnI-^{2}FnII (*A*), ^{1}FnII-^{2}FnII (*B*), and $^{1-2}$FnII-^{7}FnI (*C*).** Individual domains are colored as in Fig. 1, and specific residues are shown as *sticks* colored similar to their respective domains. Compared with the solution structure of ^{6}FnI$^{1-2}$FnII (12) a new ^{1}FnII-^{2}FnII interface (*B*) is formed, and the ^{2}FnII-^{7}FnI linker is stabilized. ^{7}FnI interacts with both ^{1}FnII and ^{2}FnII and is further anchored to this linker.

Crystallographic versus Solution ^{6}FnI$^{1-2}$FnII^{7}FnI Conformation—To evaluate whether the ^{6}FnI$^{1-2}$FnII^{7}FnI conformation observed is present in solution, we compared the NMR chemical shifts of ^{6}FnI$^{1-2}$FnII with those of ^{6}FnI$^{1-2}$FnII^{7}FnI under the same experimental conditions. Addition of ^{7}FnI to the fragment causes chemical shift differences that extend further than the immediate attachment point (*i.e.* the C terminus of ^{2}FnII; see supplemental Fig. 2). Fig. 3, *C* and *D*, shows residues whose NMR resonances differ by more than 1

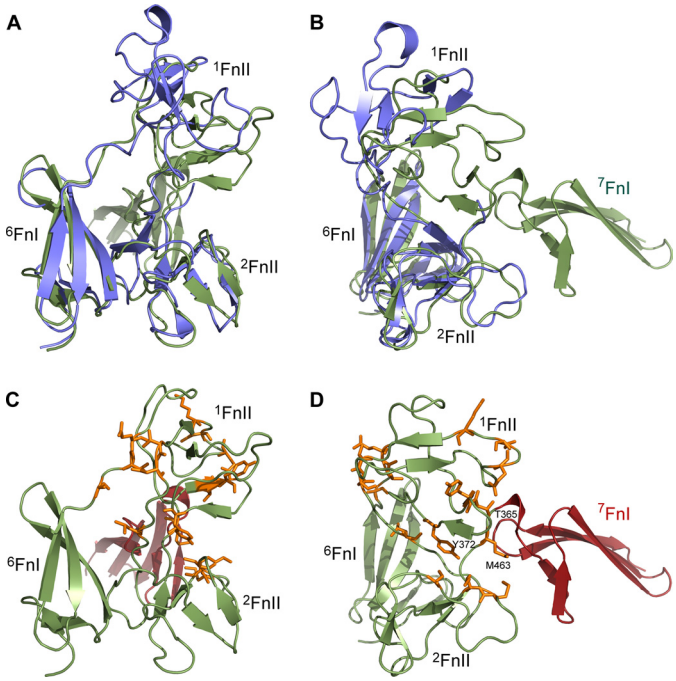

FIGURE 3. *A* and *B*, comparison of ^{6}FnI$^{1-2}$FnII^{7}FnI (*green*) with the solution structure of ^{6}FnI$^{1-2}$FnII (12) (*blue*) in two orientations. ^{1}FnII is mobile with respect to ^{6}FnI-^{2}FnII in the structure of ^{6}FnI$^{1-2}$FnII; only the best model of the ensemble (Protein Data Bank code 1E88) corresponding to approximately the average position is used. Addition of ^{7}FnI to the fragment restricts ^{1}FnII mobility through interdomain interactions. *C* and *D*, comparison of ^{6}FnI$^{1-2}$FnII *vs.* ^{6}FnI$^{1-2}$FnII^{7}FnI chemical shifts. Domains ^{6}FnI$^{1-2}$FnII are shown in *green*, and domain ^{7}FnI is in *red*. Residues with chemical shifts that differ by more than 1 S.D. compared with the average are shown in *orange*. Most affected residues are clustered around ^{7}FnI in (*D*); important interfacial residues are labeled.

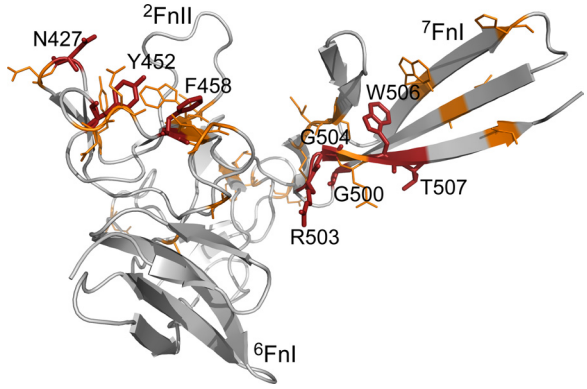

FIGURE 4. **^{6}FnI$^{1-2}$FnII^{7}FnI residues perturbed by single-stranded α_1(I) Gly^{778}-Gly^{799} binding.** Residues with chemical shift perturbations larger than 2 S.D. compared with the average are shown in *red* and are labeled. Residues perturbed between 1 and 2 S.D. are shown in *orange*. The most prominent changes upon binding occur in domains ^{2}FnII^{7}FnI and form a plausible, continuous interaction surface.

S.D. compared with the average; these include: residues at the ^{6}FnI$^{1-2}$FnII interdomain linkers (Ala^{346}, Thr^{348}, Gln^{349}, Thr^{402}, Asp^{403}, and Leu^{407}); residues at the new ^{1}FnII-^{2}FnII interface (Tyr^{372}, Cys^{434}) and numerous residues on both ^{1}FnII and ^{2}FnII that circumscribe the ^{7}FnI anchoring point (Fig. 3*D*). These differences correlate well with differences between the solution ^{6}FnI$^{1-2}$FnII structure and our model and are likely to report on the structural changes induced by the addition of ^{7}FnI to the construct. Comparison of heteronuclear {^{1}H}-^{15}N NOE data, which report on fast time scale NMR dynamics, between ^{6}FnI$^{1-2}$FnII (12) at 25 °C and ^{6}FnI$^{1-2}$FnII^{7}FnI at 37 °C (supplemental Fig. 3) shows moderate stabilization of both ^{6}FnI-^{1}FnII and ^{1}FnII-^{2}FnII loops in the larger construct. Specifically, the lowest {^{1}H}-^{15}N NOE values observed in these loops are 0.4 and 0.5, respectively, for ^{6}FnI$^{1-2}$FnII, whereas the equivalent values for ^{6}FnI$^{1-2}$FnII^{7}FnI are 0.52 and 0.68. For reference, {^{1}H}-NOE values below 0.6–0.65 typically denote flexible residues (33). Thus, although a measure of flexibility remains in ^{6}FnI$^{1-2}$FnII^{7}FnI we argue that the compact conformation seen in the crystal structure is also present in solution.

^{6}FnI$^{1-2}$FnII^{7}FnI Interactions with Collagen Peptides—Previously, we reported that a single-stranded peptide derived from the collagen α_1(I) chain, spanning residues Gly^{778}-Gly^{799} (GQRGVVGLOGQRGERGFOGLOG), interacts with ^{6}FnI$^{1-2}$FnII^{7}FnI with a $K_d \sim 60$ μM at 37 °C (7). NMR spectra under near physiological conditions showed significant chemical shift perturbations over a large number of residues, indicating an extensive binding surface. The interaction time scale was estimated to be in the microsecond range based on spectral properties. However, the lack of sequential assignments and a structural model for ^{6}FnI$^{1-2}$FnII^{7}FnI prevented further analysis of these data at the time.

As shown in supplemental Fig. 2, chemical shift perturbations larger than 2 S.D. compared with the average (*red bars*) localize exclusively on residues of ^{2}FnII^{7}FnI, and smaller but significant perturbations (1–2 S.D., *yellow bars*) largely follow the same pattern. Mapping these perturbations on the ^{6}FnI$^{1-2}$FnII^{7}FnI structure shows a dominant interaction surface (Fig. 4) spanning domains ^{2}FnII^{7}FnI and primarily involving residues Asn^{427}, Tyr^{452}, Phe^{458}, Gly^{500}, Arg^{503}, Gly^{504}, Trp^{506}, and Thr^{507}. Although ^{1}FnII does not participate in this interaction interface it stabilizes the ^{7}FnI orientation thereby contributing to the formation of a continuous ^{2}FnII^{7}FnI binding surface.

Our previous study of collagen peptides binding to GBD fragments (7) and work since then have identified α_1(I) residues Gly^{778}-Gly^{799} as the single-stranded peptide with the highest known affinity for ^{6}FnI$^{1-2}$FnII^{7}FnI in type I collagen. This peptide is adjacent to the matrix metalloproteinase 1 cleavage site and coincides with the collagen fragment implicated in FN binding using fluorescent probes (6) as well as competition assays between serum FN and collagen (34). Several other peptides are known to bind with low affinity, with K_d values of well over 1 mM (7), but these tend to cause few chemical shift perturbations. Analysis of these weak interactions showed effects primarily on Trp^{385} (^{1}FnII), Trp^{445} (^{2}FnII), and residues in their vicinity. These residues belong to a hydrophobic pocket on the surface of FnII-type modules that is known to interact weakly with collagen-like peptides (14, 35); in our crystallographic model the same sites are occupied by two 2-methyl-2,4-pentanediol molecules from the crystallization solution. We believe that these lower affinity interactions correspond to nonspecific binding events, possibly related to the generic gelatin affinity displayed by many FnII-type modules (36–38). In contrast, our higher affinity α_1(I) Gly^{778}-Gly^{799} peptide interacts with a unique interface involving only one of these two hydrophobic pockets; the peptide is likely to be a specific ligand.

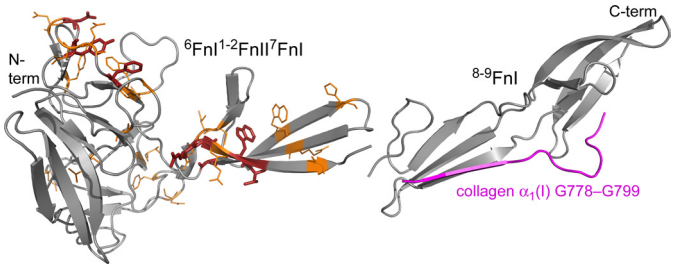

FIGURE 5. **Model of the fibronectin GBD.** ^{6}FnI$^{1-2}$FnII^{7}FnI is shown with collagen-binding residues marked as in Fig. 4, $^{8-9}$FnI is shown in complex with a single-stranded collagen peptide (*magenta*) (7), and the ^{7}FnI-^{8}FnI conformation is based on available crystallographic and solution structures of FnI domain pairs (7,29,32,39). The N and C termini of the model are indicated as *N-* and *C-term*. The peptide-binding residues of ^{6}FnI$^{1-2}$FnII^{7}FnI and the collagen peptide bound to $^{8-9}$FnI form a continuous interaction site.

To test whether native-like, triple-helical peptides interact with ^{6}FnI$^{1-2}$FnII^{7}FnI in a similar fashion, we performed NMR titrations using a synthetic peptide based on the homotrimeric collagen type II sequence. This fragment, spanning residues Gly^{775}-Ser^{801} of the α_1(II) chain (GPC(GPP)$_5$GLAGQRGIVG-LOGQRGERGFOGLOGPS(GPP)$_5$GPC), is highly homologous to our high affinity α_1(I) peptide and includes the matrix metalloproteinase 1 cleavage site. Previous work (7, 23), and CD data shown here (supplemental Fig. 4) confirm that this peptide adopts a stable triple-helical conformation at room temperature. NMR spectra of ^{6}FnI$^{1-2}$FnII^{7}FnI with this peptide at 25 °C and 950 MHz ^{1}H frequency (supplemental Fig. 5) show extensive line broadening for many residues. Varying the temperature between 15 and 37 °C did not produce a marked difference in spectral appearance. Control titrations using (GPP)$_{10}$ triple-helical peptides did not show broadening of ^{6}FnI$^{1-2}$FnII^{7}FnI residues under the same conditions (data not shown). Mapping the most affected resonances on the primary sequence (supplemental Fig. 1) produces an image that is qualitatively similar to that of the interaction with the single-stranded peptide, with the vast majority of perturbations seen on domains ^{2}FnII and ^{7}FnI. Compared with the single-stranded peptide, the line broadening observed here indicates that this interaction probably occurs in a slower time scale (microseconds to milliseconds). Spectral broadening prevented us from measuring an affinity value for this peptide by NMR.

GBD Modeling and Interactions with Long Collagen Peptides—Previously, we showed that NMR spectra of the GBD overlay well with spectra of the individual ^{6}FnI$^{1-2}$FnII^{7}FnI and $^{8-9}$FnI subfragments, especially in the presence of collagen peptides (7). This overlay indicates that the GBD structure does not feature radical rearrangement of domains compared with the subfragments. Rather, the GBD is likely to comprise a linear combination of ^{6}FnI$^{1-2}$FnII^{7}FnI and $^{8-9}$FnI connected through the $^{7-8}$FnI interface. We reconstructed this missing interface using the relative FnI domain orientation observed in almost all structures of FnI-domain pairs (7, 29, 32, 39) as guidance; the resulting GBD model is presented in Fig. 5. We predict that the GBD will adopt an elongated conformation of ~100 Å across the longest axis and ~35 Å maximal width at the ^{6}FnI$^{1-2}$FnII base. The overall chain direction between ^{6}FnI and ^{9}FnI differs by ~90°, a significant change compared with the GBD hairpin models previously considered (12). As seen in Fig. 5, the $^{8-9}$FnI-bound collagen peptide (7) is co-linear with the collagen binding interface in ^{6}FnI$^{1-2}$FnII^{7}FnI, indicating the presence of a single continuous binding surface. $^{8-9}$FnI binds collagen in an antiparallel orientation; the last collagen residue interacting with $^{8-9}$FnI is Arg^{792} of α_1(I), which suggests that residues C-terminal to Arg^{972} would bind ^{6}FnI$^{1-2}$FnII^{7}FnI. However, isolated peptides spanning α_1(I) residues Gly^{796}-Arg^{816} interact with ^{6}FnI$^{1-2}$FnII^{7}FnI only very weakly as judged by NMR (7).

To test whether ^{6}FnI$^{1-2}$FnII^{7}FnI and $^{8-9}$FnI can bind collagen in a concerted fashion in the context of the GBD, we performed ITC experiments using GBD, $^{8-9}$FnI, and a long peptide, α_1(I) residues Gly^{778}-Arg^{816}. This peptide includes the high affinity $^{8-9}$FnI epitope and extends to potentially cover the ^{6}FnI$^{1-2}$FnII^{7}FnI collagen binding surface observed here (Fig. 4). Although this peptide was not designed to form triple helices, a degree of helical structure was detected by CD at conditions similar to those used for ITC (supplemental Fig. 4). The partial helical structure of α_1(I) Gly^{778}-Arg^{816} may impede $^{8-9}$FnI binding as it will necessitate peptide unwinding and adoption of an extended conformation prior to interaction (7). As seen in supplemental Fig. 6, $^{8-9}$FnI binds α_1(I) Gly^{778}-Arg^{816} with relatively weak affinity (K_d ~115 μM). However, under the same conditions, GBD bound α_1(I) Gly^{778}-Arg^{816} ~3 times more tightly. Although the increase in affinity is moderate, it is in agreement with our model for concerted binding of the two GBD subfragments to collagen.

DISCUSSION

$^{8-9}$FnI was previously shown to interact tightly (K_d ~5 μM) with a specific collagen peptide derived from the α_1(I) chain (7). Crystallographic analysis of this complex also allowed us to identify a number of putative sites for $^{8-9}$FnI on that chain. The role of ^{6}FnI$^{1-2}$FnII^{7}FnI in the GBD, however, remained unknown. Here, we presented the crystal structure of ^{6}FnI$^{1-2}$FnII^{7}FnI, which together with the structure of $^{8-9}$FnI (7) and extensive NMR titration analysis allowed us to model the structure of the full GBD of FN. Our results offer new insights into how FN may interact with collagen.

GBD adopts an elongated structure in our model in which the two spatially distinct subfragments show good binding to the same collagen type I sequence, residues Gly^{788}-Gly^{799}. A question thus emerges as to how both ^{6}FnI$^{1-2}$FnII^{7}FnI and $^{8-9}$FnI can associate with the same epitope. Previous hypotheses included GBD binding to two of the three strands in a single triple helix, or GBD associating with multiple strands across the collagen microfibril (7). However, neither of these hypotheses is plausible as they would necessitate collagen chain displacements beyond the local fluctuations believed to be present under physiological conditions (40).

An alternative hypothesis emerges from our GBD model and the ITC data: a continuous collagen binding site on GBD can interact with a single long collagen epitope in a concerted fashion. Although the available evidence is tentative, the interplay between the two GBD subfragments in binding collagen chains could facilitate tight attachment. It is intriguing to speculate on the relative contributions of the GBD subfragments to such a binding event. ^{6}FnI$^{1-2}$FnII^{7}FnI was shown here, and earlier (7), to form relatively weak, transient complexes with single-

stranded and triple-helical forms of collagen peptides; in contrast $^{8-9}$FnI binds more tightly to unwound collagen strands. There is a growing body of evidence that weak, transient encounter complexes precede formation of tight intermolecular complexes in biological systems (41, 42). Thus, it is possible that ^{6}FnI$^{1-2}$FnII^{7}FnI binds adjacent to the collagenase site and shifts the local fluctuations of the collagen triple helix toward the unwound state (40, 43–45); this state is then bound tightly by $^{8-9}$FnI. Indeed, our ITC data suggest that the complete GBD can bind partly helical collagen peptides better than $^{8-9}$FnI.

Recently, Graille *et al.* determined the crystallographic structure of the GBD in the presence of millimolar level concentrations of Zn^{2+} (46). Under these conditions GBD forms a compact homodimer in which domain ^{8}FnI loses the canonical FnI fold; instead ^{8}FnI forms β-strand extension-type interactions with domains ^{7}FnI and ^{9}FnI. Experiments with fluorescently labeled collagen peptides showed that Zn^{2+} at concentrations of hundreds of micromolar interferes with collagen binding by the GBD. These concentrations are much higher than the physiological levels of Zn^{2+} in blood, 10–15 μM (47–49), although Zn^{2+} levels may be higher locally in specific tissues. Thus, Zn^{2+} could play a regulatory role in the FN-collagen interaction through conformational changes; in this case the GBD model we propose here would correspond to the collagen binding form of FN.

The role of FN-collagen binding *in vivo* has been assessed over many years; putative FN roles include scavenging of collagen fragments (50–52), stabilization and protection of collagen fibrils (4), and acting as a molecular tag for collagen proteolysis. FN has also been reported to be an opsonic protein (53, 54), enhancing phagocytosis when bound to a target. Numerous examples of FN localization to damaged tissue are known, including localization to burned skin as well as injured liver (50, 55–57). Given the ubiquitous distribution of FN in the extracellular matrix as well as in plasma, we believe that the FN-collagen interaction may serve more than one purpose. Considering the widespread interest in extracellular matrix components and their interactions in the field of biomaterials and prosthetics (58, 59), our structural data may have significant influence on future biotechnological as well as medical studies.

Acknowledgments—We thank Drs. Vincent Olieric and Meitian Wang for help with at the SLS crystallographic beamline and Nick Soffe and Dr. Jonathan Boyd for upkeep of the Oxford Biochemistry NMR instrumentation.

REFERENCES

1. Leitinger, B., and Hohenester, E. (2007) *Matrix Biol.* **26,** 146–155
2. Orgel, J. P., Irving, T. C., Miller, A., and Wess, T. J. (2006) *Proc. Natl. Acad. Sci. U.S.A.* **103,** 9001–9005
3. Holmes, D. F., and Kadler, K. E. (2006) *Proc. Natl. Acad. Sci. U.S.A.* **103,** 17249–17254
4. Kadler, K. E., Hill, A., and Canty-Laird, E. G. (2008) *Curr. Opin. Cell Biol.* **20,** 495–501
5. Vakonakis, I., and Campbell, I. D. (2007) *Curr. Opin. Cell Biol.* **19,** 578–583
6. Ingham, K. C., Brew, S. A., and Isaacs, B. S. (1988) *J. Biol. Chem.* **263,** 4624–4628
7. Erat, M. C., Slatter, D. A., Lowe, E. D., Millard, C. J., Farndale, R. W., Campbell, I. D., and Vakonakis, I. (2009) *Proc. Natl. Acad. Sci. U.S.A.* **106,** 4195–4200
8. Fields, G. B. (1991) *J. Theor. Biol.* **153,** 585–602
9. Ingham, K. C., Landwehr, R., and Engel, J. (1985) *Eur. J. Biochem.* **148,** 219–224
10. Nagase, H., and Fields, G. B. (1996) *Biopolymers* **40,** 399–416
11. Leikina, E., Mertts, M. V., Kuznetsova, N., and Leikin, S. (2002) *Proc. Natl. Acad. Sci. U.S.A.* **99,** 1314–1318
12. Pickford, A. R., Smith, S. P., Staunton, D., Boyd, J., and Campbell, I. D. (2001) *EMBO J.* **20,** 1519–1529
13. Katagiri, Y., Brew, S. A., and Ingham, K. C. (2003) *J. Biol. Chem.* **278,** 11897–11902
14. Pagett, A., Campbell, I. D., and Pickford, A. R. (2005) *Biochemistry* **44,** 14682–14687
15. Vakonakis, I., Langenhan, T., Prömel, S., Russ, A., and Campbell, I. D. (2008) *Structure* **16,** 944–953
16. Sauter, N. K., Grosse-Kunstleve, R. W., and Adams, P. D. (2004) *J. Appl. Crystallogr.* **37,** 399–409
17. Kabsch, W. (2010) *Acta Crystallogr. D. Biol. Crystallogr.* **66,** 125–132
18. Evans, P. (2006) *Acta Crystallogr. D. Biol. Crystallogr.* **62,** 72–82
19. Adams, P. D., Grosse-Kunstleve, R. W., Hung, L. W., Ioerger, T. R., McCoy, A. J., Moriarty, N. W., Read, R. J., Sacchettini, J. C., Sauter, N. K., and Terwilliger, T. C. (2002) *Acta Crystallogr. D. Biol. Crystallogr.* **58,** 1948–1954
20. Zwart, P. H., Afonine, P. V., Grosse-Kunstleve, R. W., Hung, L. W., Ioerger, T. R., McCoy, A. J., McKee, E., Moriarty, N. W., Read, R. J., Sacchettini, J. C., Sauter, N. K., Storoni, L. C., Terwilliger, T. C., and Adams, P. D. (2008) *Methods Mol. Biol.* **426,** 419–435
21. Emsley, P., and Cowtan, K. (2004) *Acta Crystallogr. D Biol. Crystallogr.* **60,** 2126–2132
22. Davis, I. W., Leaver-Fay, A., Chen, V. B., Block, J. N., Kapral, G. J., Wang, X., Murray, L. W., Arendall, W. B., 3rd, Snoeyink, J., Richardson, J. S., and Richardson, D. C. (2007) *Nucleic Acids Res.* **35,** W375–W383
23. Konitsiotis, A. D., Raynal, N., Bihan, D., Hohenester, E., Farndale, R. W., and Leitinger, B. (2008) *J. Biol. Chem.* **283,** 6861–6868
24. Raynal, N., Hamaia, S. W., Siljander, P. R., Maddox, B., Peachey, A. R., Fernandez, R., Foley, L. J., Slatter, D. A., Jarvis, G. E., and Farndale, R. W. (2006) *J. Biol. Chem.* **281,** 3821–3831
25. Vakonakis, I., Staunton, D., Rooney, L. M., and Campbell, I. D. (2007) *EMBO J.* **26,** 2575–2583
26. Yamazaki, T., Forman-Kay, J. D., and Kay, L. E. (1993) *J. Am. Chem. Soc.* **115,** 11054–11055
27. DeLano, W. L. (2002) *The PyMOL Molecular Graphics System*, DeLano Scientific LLC, San Carlos, CA
28. Krissinel, E., and Henrick, K. (2007) *J. Mol. Biol.* **372,** 774–797
29. Bingham, R. J., Rudiño-Piñera, E., Meenan, N. A., Schwarz-Linek, U., Turkenburg, J. P., Höök, M., Garman, E. F., and Potts, J. R. (2008) *Proc. Natl. Acad. Sci. U.S.A.* **105,** 12254–12258
30. Wishart, D. S., Sykes, B. D., and Richards, F. M. (1992) *Biochemistry* **31,** 1647–1651
31. Leahy, D. J., Aukhil, I., and Erickson, H. P. (1996) *Cell* **84,** 155–164
32. Rudiño-Piñera, E., Ravelli, R. B., Sheldrick, G. M., Nanao, M. H., Korostelev, V. V., Werner, J. M., Schwarz-Linek, U., Potts, J. R., and Garman, E. F. (2007) *J. Mol. Biol.* **368,** 833–844
33. LiWang, A. C., Cao, J. J., Zheng, H., Lu, Z., Peiper, S. C., and LiWang, P. J. (1999) *Biochemistry* **38,** 442–453
34. Kleinman, H. K., Wilkes, C. M., and Martin, G. R. (1981) *Biochemistry* **20,** 2325–2330
35. Xu, X., Mikhailova, M., Ilangovan, U., Chen, Z., Yu, A., Pal, S., Hinck, A. P., and Steffensen, B. (2009) *Biochemistry* **48,** 5822–5831
36. Gehrmann, M. L., Douglas, J. T., Bányai, L., Tordai, H., Patthy, L., and Llinás, M. (2004) *J. Biol. Chem.* **279,** 46921–46929
37. Trexler, M., Briknarová, K., Gehrmann, M., Llinás, M., and Patthy, L. (2003) *J. Biol. Chem.* **278,** 12241–12246
38. Hornebeck, W., Bellon, G., and Emonard, H. (2005) *Pathol. Biol.* **53,** 405–410
39. Schwarz-Linek, U., Werner, J. M., Pickford, A. R., Gurusiddappa, S., Kim,

J. H., Pilka, E. S., Briggs, J. A., Gough, T. S., Höök, M., Campbell, I. D., and Potts, J. R. (2003) *Nature* **423,** 177–181
40. Perumal, S., Antipova, O., and Orgel, J. P. (2008) *Proc. Natl. Acad. Sci. U.S.A.* **105,** 2824–2829
41. Fawzi, N. L., Doucleff, M., Suh, J. Y., and Clore, G. M. (2010) *Proc. Natl. Acad. Sci. U.S.A.* **107,** 1379–1384
42. Tang, C., Ghirlando, R., and Clore, G. M. (2008) *J. Am. Chem. Soc.* **130,** 4048–4056
43. Chung, L., Dinakarpandian, D., Yoshida, N., Lauer-Fields, J. L., Fields, G. B., Visse, R., and Nagase, H. (2004) *EMBO J.* **23,** 3020–3030
44. Fiori, S., Saccà, B., and Moroder, L. (2002) *J. Mol. Biol.* **319,** 1235–1242
45. Stultz, C. M. (2002) *J. Mol. Biol.* **319,** 997–1003
46. Graille, M., Pagano, M., Rose, T., Ravaux, M. R., and van Tilbeurgh, H. (2010) *Structure* **18,** 710–718
47. Fallah, S., Sani, F. V., and Firoozrai, M. (2009) *Contraception* **80,** 40–43
48. Iyengar, V., and Woittiez, J. (1988) *Clin. Chem.* **34,** 474–481
49. Versieck, J. (1985) *Crit. Rev. Clin. Lab. Sci.* **22,** 97–184
50. La Celle, P., Blumenstock, F. A., McKinley, C., Saba, T. M., Vincent, P. A., and Gray, V. (1990) *Blood* **75,** 470–478
51. Blumenstock, F. A., La Celle, P., Herrmannsdoerfer, A., Giunta, C., Minnear, F. L., Cho, E., and Saba, T. M. (1993) *J. Leukocyte Biol.* **54,** 56–64
52. Di Lullo, G. A., Sweeney, S. M., Korkko, J., Ala-Kokko, L., and San Antonio, J. D. (2002) *J. Biol. Chem.* **277,** 4223–4231
53. Blumenstock, F. A., Saba, T. M., Weber, P., and Laffin, R. (1978) *J. Biol. Chem.* **253,** 4287–4291
54. Kaplan, J. E., Molnar, J., Saba, T. M., and Allen, C. (1976) *J. Reticuloendothel. Soc.* **20,** 375–384
55. Deno, D. C., McCafferty, M. H., Saba, T. M., and Blumenstock, F. A. (1984) *J. Clin. Invest.* **73,** 20–34
56. Eriksen, H. O., Kalaja, E., Jensen, B. A., and Clemmensen, I. (1984) *Burns Incl. Therm. Inj.* **10,** 422–426
57. Lanser, M. E., Saba, T. M., and Scovill, W. A. (1980) *Ann. Surg.* **192,** 776–782
58. Metcalfe, A. D., and Ferguson, M. W. (2007) *J. R. Soc. Interface* **4,** 413–437
59. van den Dolder, J., Bancroft, G. N., Sikavitsas, V. I., Spauwen, P. H., Mikos, A. G., and Jansen, J. A. (2003) *Tissue Eng.* **9,** 505–515